TTU-ES-70-4

A PHOTOELASTIC INVESTIGATION OF STRESS WAVE LOADING OF A CRACK

by

DALLAS G. SMITH

Prepared For

NATIONAL AERONAUTICS AND SPACE ADMINISTRATION

MANNED SPACECRAFT CENTER

HOUSTON, TEXAS

GRANT NUMBER NGR 43-003-007

SEPTEMBER, 1970

TENNESSEE TECHNOLOGICAL UNIVERSITY

DEPARTMENT OF ENGINEERING SCIENCE

COOKEVILLE, TENNESSEE 38501

TTU-ES-70-4

A PHOTOELASTIC INVESTIGATION OF STRESS WAVE LOADING OF A CRACK

by

DALLAS G. SMITH

Prepared For

NATIONAL AERONAUTICS AND SPACE ADMINISTRATION

MANNED SPACECRAFT CENTER

HOUSTON, TEXAS

Grant Number NGR 43-003-007

SEPTEMBER, 1970

TENNESSEE TECHNOLOGICAL UNIVERSITY

DEPARTMENT OF ENGINEERING SCIENCE

COOKEVILLE, TENNESSEE 38501

A PHOTOELASTIC INVESTIGATION OF STRESS WAVE LOADING OF A CRACK

The photoelastic determination of the dynamic stress-intensity factor for five different crack length to pulse length ratios

by

Dallas G. Smith

Assistant Professor of Engineering Science
Tennessee Technological University
Cookeville, Tennessee

ABSTRACT - Using a photoelastic technique the dynamic stress-intensity factor for the wave loading of a crack is investigated, and the dynamic polariscope is described. Five different crack lengths were considered and the pulse length was approximately constant. The dilatational wave impinged normal to the crack and the form of the incident wave was determined. The time response of the stress-intensity factor is shown for each crack length and the effect of the crack length to pulse length ratio on the maximum stress intensity is presented.

INTRODUCTION

Recently in the field of fracture mechanics considerable work has been devoted to solving the problem of a crack subjected to a stress wave loading. Most notable among these has been the work of Sih and Loeber[1,2,3,4]. For finite plane cracks and penny-shaped cracks subjected to various harmonic wave loadings, they have found the spatial distribution of stresses near the crack tip to be the same as the static case and they have defined a dynamic stress-intensity factor which reduces to the static value for the case of a very high wave length to crack length ratio. In the theory of brittle fracture the stress-intensity factor governs the onset of unstable crack propagation. Their results show that for certain values of the crack length to wave length ratio the stress-intensity factor is significantly higher than the static value. Recently Ravera and Sih[5] solved the problem of a finite crack opened suddenly by anti-plane strain shear forces. Their results show that the dynamic stress-intensity factor increases to a value approximately 50% larger than the static value and then oscillates in time about the static value and eventually approaches the static value for large time. Jahanshahi[6] and Mal[7] have also contributed steady state examples. Further references are given by Sih[8].

No solution to date, however, has presented the transient stress-intensity for the important case of a dilatational wave impinging on a finite crack; the solution of this problem appears fraught with mathematical difficulty. Since this is physically a commonly occurring case, it was decided to try to measure the stress-intensity factor, using dynamic photoelasticity, for normal wave incidence on cracks of various lengths. The information gained may be useful in explaining fractures and spallations due to pulses caused by hypervelocity impact such as reported by Kinslow[9].

THEORETICAL CONSIDERATIONS

Figure 1 shows a dilatational stress pulse impinging at normal incidence on a plane crack. For the interval $0 < t \ \frac{a}{c_1}$, where t is time a is the half crack length, and c_i is the velocity of a dilatational wave, the following zones can be identified (See, for instance, Miles[10] and Flitman[11]):

- I - incidence pulse zone
- II - geometric reflection
- III - shadow zone
- IV - dilatational wave scattering zone
- V - shear wave scattering zone

For $\frac{a}{c_1} < t \leq \frac{2a}{c_1}$ the scattered dilatational waves radiating from the two crack tips come together and interact, as do the scattered shear waves for $\frac{a}{c_2} < t \leq \frac{2a}{c_2}$. For $\frac{2a}{c_1} < t \leq \frac{4a}{c_1}$ and $\frac{2a}{c_2} < t \leq \frac{4a}{c_2}$ the scattered dilatational waves and scattered shear waves respectively reach the opposite crack tip and slide off, generating in turn new crack-tip waves of lesser magnitude. For larger time this type of interaction continues, and the stress field near the crack is obviously very complicated.

To allow a quantitative evaluation of the stress-intensity at the crack tips for use in the theory of brittle fracture, the following assumptions are employed: (1) The stresses associated with the scattered shear wave are negligible in comparison with the stresses associated with the dilatational wave. In the theory of fracture this is comparable to ignoring the small amount of mode II deformation. (2) The stresses due to the second generation of scattered waves are small. The validity of these two assumptions--at least qualitatively--was borne out by the experiment. (3) The plane stresses due to the scattered dilatational wave are assumed to take the form,

$$\begin{aligned}
\sigma_{xx}^{s} &= \frac{K_1}{(2r)^{1/2}} \cos\frac{\theta}{2}\left[1 - \sin\frac{\theta}{2}\sin\frac{3\theta}{2}\right] + 0(1) \\
\sigma_{yy}^{s} &= \frac{K_1}{(2r)^{1/2}} \cos\frac{\theta}{2}\left[1 + \sin\frac{\theta}{2}\sin\frac{3\theta}{2}\right] + 0(1) \qquad (1) \\
\sigma_{xy}^{s} &= \frac{K_1}{(2r)^{1/2}} \cos\frac{\theta}{2}\sin\frac{\theta}{2}\cos\frac{3\theta}{2} + 0(1)
\end{aligned}$$

where the superscript denotes "scattered" and the crack tip coordinates θ and r are shown in Figure 1. K_1 is the familiar mode I stress intensity factor, which here varies with time. The distribution in θ, which is the same as in the static case, has been determined by Sih and Loeber[3] for the normal incidence of a harmonic dilatational wave. Also for the transient case of a crack loaded suddenly in anti-plane strain Ravera and Sih[5] have shown that the distribution in θ is the same as in the static case up until the wave fronts interact.

Considering the region $-\frac{\pi}{2} < \theta < +\frac{\pi}{2}$ (due to the specular reflection a discontinuity exists at $\theta = \pm\frac{\pi}{2}$) and $r \leq c_1 t$ and superposing the scattered stresses onto the incident stresses, σ_{xx}^{i} and σ_{yy}^{i} ($\sigma_{xy}^{i} = 0$), the following is obtained for the total stresses near the crack tip.

$$\begin{aligned}
\sigma_{xx}^{t} &= \frac{K_1}{(2r)^{1/2}} \cos\frac{\theta}{2}\left[1 - \sin\frac{\theta}{2}\sin\frac{3\theta}{2}\right] + \sigma_{xx}^{i} + 0(1) \\
\sigma_{yy}^{t} &= \frac{K_1}{(2r)^{1/2}} \cos\frac{\theta}{2}\left[1 + \sin\frac{\theta}{2}\sin\frac{3\theta}{2}\right] + \sigma_{yy}^{i} + 0(1) \qquad (2) \\
\sigma_{xy}^{t} &= \frac{K_1}{(2r)^{1/2}} \cos\frac{\theta}{2}\sin\frac{\theta}{2}\cos\frac{3\theta}{2} + 0(1)
\end{aligned}$$

Neglecting terms of $O(1)$ (which should be valid for $r/a \leq 0.1$) and using the formula

$$\tau_m = \pm\sqrt{\left(\frac{\sigma_{xx}-\sigma_{yy}}{2}\right)^2 + \sigma_{xy}^{\;2}} \tag{3}$$

for the maximum in-plane, shear stress, the expected shape of the isochromatics near the crack tip is found to be,

$$(\tau_m^t)^2 = \left[\frac{K_1}{2(2r)^{1/2}}\sin\theta + \frac{\sigma_{yy}^i-\sigma_{xx}^i}{2}\sin\frac{3\theta}{2}\right]^2 + \left[\frac{\sigma_{yy}^i-\sigma_{xx}^i}{2}\cos\frac{3\theta}{2}\right]^2 \tag{4}$$

This can be written in terms of the photoelastic fringe order by the use of

$$\frac{\sigma_{yy}^i-\sigma_{xx}^i}{2} = \frac{F_\sigma N^i}{2h} \tag{5}$$

and

$$\tau_m^t = \frac{F_\sigma N^t}{2h} \tag{6}$$

where F_σ is the material stress-fringe constant, h is the plate thickness, and N^i and N^t are the incident and the total fringe order respectively. The quantity N^t can be measured near the crack, and N^i can be measured at a point on the incident wave front corresponding to the location of the crack tip but remote from the actual crack tip. Such a procedure circumvents the need for determination of the fringe constant F_σ. It is convenient to represent K_1 as

$$K_1 = g(2a/L;t)\,(\sigma_{yy}^i)_0\,a^{1/2} \tag{7}$$

where $g(2a/L;t)$, a measure of the dynamic effect, varies in time and depends on the crack-length to pulse length ratio $2a/L$, where L is a characteristic length of the pulse. The static value of the stress-intensity factor is $(\sigma_{yy}^i)_0\,a^{1/2}$ for a remote loading of $(\sigma_{yy}^i)_0$ normal to the crack. The quantity $(\sigma_{yy}^{i})_0$ can be determined photoelastically as, some number, say N, times F_σ/h, i.e.

$$(\sigma_{yy}^{i})_0 = N \frac{F_\sigma}{h} \tag{8}$$

Finally putting (5) and (6) together with (7) and (8) into (4) and rearranging, the following useful form is obtained for determining g(2a/L;t)

$$g(2a/L;t) = \frac{\sqrt{2\bar{r}}}{N\sin\theta}\left[\sqrt{(N^t)^2 - (N^i \cos\frac{3\theta}{2})^2} - N^i \sin\frac{3\theta}{2}\right] \tag{9}$$

where $\bar{r} = r/a$. Corresponding to various values of r and θ the quantities N^t, N^i, and N can be measured by photoelasticity and g(2a/L;t) determined, thus yielding the dynamic stress-intensity factor. This is similar to a technique used before by Smith and Smith.[12]

THE EXPERIMENTS

The Incident Wave

Because of the difficulty of making a reproducible wave with a plane front as shown in Figure 1, it was decided to use a cylindrical wave emanating from the edge of a plate at a point sufficiently remote from the crack that the curvature of the front upon reaching the crack was small. Further, the pulse used was a compressive pulse instead of the more important tensile pulse. A compressive pulse, however, can be used to simulate a tensile pulse if interference of the crack surfaces is prevented, as was done in this study. Figure 2 shows the location of the crack in the plate and the origin of the cylindrical wave. The crack is located a distance of 5 inches from the origin of the wave, and a free point was selected at an equal distance from the origin, symmetric with the crack tip about the centerline of the plate. Until the disturbance due to the crack reaches the free point, the stresses determined at the free point represent the loading imposed on the crack. This is similar to a technique used before by Durelli and Riley.[13] The incident wave is cylindrical over a wide portion of its front. Since a dilatational wave propagates without rotation, deformations occur only in the R direction, and the displacements and stresses are independent of Θ. For this case, using a method described by Dally and Riley[14], it is possible to determine the individual stresses from the fringe orders alone. The stresses are determined by numerical integration according to:

$$\sigma_R = -\left(\frac{1}{1-\nu}\right)\frac{F_\sigma}{h}\left[N^i + (1+\nu)\int\frac{N^i}{R}\,dR\right]$$
$$\sigma_\Theta = -\left(\frac{1}{1-\nu}\right)\frac{F_\sigma}{h}\left[\nu N^i + (1+\nu)\int\frac{N^i}{R}\,dR\right] \qquad (10)$$

where N^i is the fringe order of the incident wave, ν is Poisson's ratio, F_σ is the photoelastic fringe constant, and h is the plate thickness. A computer program[15] has been written to perform this integration so that the loading history of the crack is known.

The Experimental Setup

Dynamic photoelasticity has been employed before to study the related problem of dynamic crack propagation by such people as Wells and Post[16], Stock[17], and recently by Bradley and Kobayashi.[18] The polariscope used in this study has been described before by Kinslow and Delano.[19]

To record the dynamic fringe patterns a Beckman and Whitley Model 201 synchronous framing camera was used. The camera, a rotating mirror type, makes 12, 0.5 inch x 0.9 inch pictures on a 4 inch x 5 inch film at rates up to one million frames a second. At this rate the apparent exposure time is 0.6 second. A schematic diagram of the experimental setup is shown in Figure 3, and Figure 4 shows a photograph of the apparatus. The camera mirror is driven by a small gas turbine. A turbine speed of 2000 rps was used in this experiment, the rate of rotation being determined from the digital counter. Two delay generators were used to properly time the initiation of the event and the activation of the light source. The two pulse generators, which supply 100 Joules at 5 KV each, were used to supply energy to trigger the impact explosion and to activate the light source. For an intense light source a Buss type AGC-3/4 safety fuse was exploded. This provided sufficient intensity and duration to illuminate all twelve frames. A red filter was used to provide monochromatic light resulting in a circular polariscope. In some cases a neutral density filter was used at the camera to prevent over exposure.

A "gun" as indicated in Figure 2 was devised to provide the edge impact. At the bottom of a small hole, which acted as a short barrel, was placed an exploding wire on top of which was placed 16.0 mg of urea nitrate. On top of the urea nitrate was finally placed a gun primer, which, in addition to providing a small bonus explosion, acted as a projectile to initially contain the explosion and to strike the plate edge. This made a wave of sufficient amplitude, which could be reproduced very well.

The material selected for the model was a 1/4 inch thick plate of PSM-1, a clear polyester sheet manufactured by Photoelastic, Inc. This material has excellent sensitivity and freedom from time edge effects. The wave speed in this material is approximately 60,000 ips. The properties of the material given by the manufacturer are $E = 340{,}000$ psi, $F_\sigma = 40$ psi/fringe/in., $\nu = 0.38$, and $\rho = 2.36$ lb-sec^2/ft^4.

The crack was made in the model plate by drilling a hole of 0.070 inch diameter and extending a slot with a small hand-held scroll saw blade resulting in a crack approximately 0.02 inch wide. After a given test a new crack length was obtained by further extending the slot.

RESULTS AND DISCUSSION

Experimental Results

As summarized in the table below, tests were run on five different crack lengths while the pulse length was approximately constant.

Test Number	1	2	3	4	5
Crack length (2a) (in.)	0.31	0.50	0.75	1.00	1.25
Pulse length (L) (in.)	1.48	1.52	1.37	1.50	1.41
Crack length to pulse length ratio ($\frac{2a}{L}$)	0.21	0.33	0.55	0.67	0.89

The small pictures made by the rotating camera were enlarged for every other frame. As an example, the resulting sequence of pictures obtained for the 1 inch crack is shown in Figure 5. A further enlargement of one frame, shown in Figure 6, shows better the crack tip fringes and the incident fringes; the incident fringe orders are labeled.

Two shots were necessary to obtain the complete passage of the pulse. A disadvantage of the rotating mirror camera is that for a given speed of rotation the time between frames cannot be varied, and a high rate or rotation was necessary in order to shorten the apparent exposure time. Thus, with the speed used, all twelve frames were exposed before the entire compressive pulse had passed. A second shot was therefore necessary, where the timing was adjusted so that exposures started in time approximately where the first short had left off. In Figure 5 the pictures up through t = 90.5 μ sec were obtained with one shot while the pictures from t = 90.8 μ sec to t = 103.3 μ sec were obtained with a second shot. The resulting plot of fringes along a radial line through the free point, shown in Figure 7, shows the good continuity of the second wave with the first. Due to slight discrepancies in the timing it was necessary to use the measured fringe velocity from the first shot to obtain the times for the second shot.

From a plot of the fringe orders as shown in Figure 7, the stresses in the R and θ directions were obtained by numerical integration in accordance with equation (6). Near the crack the stresses σ_R and σ_Θ correspond to the incident stresses σ_{yy}^{i} and σ_{xx}^{i}, respectively, and will be referred to as such from here on. The stresses σ_{yy}^{i} and σ_{xx}^{i} are shown in Figure 8 for the various times. The stress σ_{xx}^{i} is assumed to have no effect on the stress-intensity factor but is shown for completeness. The plot of σ_{yy}^{i} shows the stress pulse which propagates onto the crack. The pulse length L is taken to be the length of the compressive portion at the front of the wave. The stress history at the free point--which may be regarded as the loading history of the crack--for all crack lengths tested is shown in Figure 9. The strain rates at the front of the wave were of the order of 10^2 in/in/sec.

The nondimensional dynamic stress-intensity factor is plotted on Figure 9 along with the crack loading history. The dynamic stress-intensity factor was calculated by the use of equation (9). Measurements were made of N^t and r near the crack tip along the lines $\theta = 70^0$ and 290^0. Crack tip measurements were only made on the tip near the center of the plate since the other tip was outside the cylindrical portion of the wave. The measurements for r were made under a magnifying glass to the nearest 0.01 inch from an actual size photograph. The values for N^i at a corresponding distance R were read from the plot of the fringe orders as shown in Figure 7. The calculations were made for successively smaller and smaller values of r down approximately to r = 0.08 inch. The results varied significantly with r, and therefore the apparent value of the stress-intensity factor was extrapolated to $r = 0$ to get a true value. This extrapolation was approximate because of data scatter and because measurements could not be made near enough to the crack tip. Based on the extrapolation error the 95% confidence limits are shown in Figure 9.

From the appearance of the crack-tip fringes very little mode II type deformation appeared present, especially near the time of maximum stress-intensity factor, as evidenced in Figure 6. According to Reference 20 the presence of mode II is indicated when the fringes on each side very near the crack tip appear to be centered about a common line at an oblique angle to the crack plane. The relative absence of this phenomenon supports the assumption of negligible mode II deformation.

Discussion of Results

Based on the dynamic stress-intensity factor shown in Figure 9, the following comments are made. During the passage of the pulse the stress intensity builds up to a peak value and then decreases much as one would expect. In all cases, however, the stress-intensity factor lags the crack loading stress. This lag is of the order 5 to 9 μ sec except for the shortest crack where the lag was only approximately 1 μ sec. After the pulse has passed and the crack loading stress has gone to zero the stress-intensity factor remains quite large and appears to reach zero a considerable time after the crack loading stress. Since the crack loading histories were all slightly different, the loading history is shown for each crack length. Also shown on each graph is the time of arrival of the scattered dilatational wave front from the opposite crack tip. This does not appear to correlate with any sudden change in the stress-intensity factor, and therefore its effect would seem to be small as assumed. The nondimensionalizing stress $(\sigma_{yy}^{i})_0$ used in Figure 9 is the peak stress the pulse has at the free point.

Figure 10 depicts how the maximum stress-intensity factor varies with 2a/L. For small values of 2a/L the maximum stress-intensity factor increases up to approximately 20% larger than the static value at 2a/L = 0.30 and then decreases down to approximately 65% of the static value at 2a/L = 0.90. For larger values of 2a/L the experimental results indicate that the maximum nondimensional stress-intensity factor continues to decrease. An interesting comparison is made with the results of Sih and Loeber[3] for the normal incidence of a steady harmonic dilatational wave with wavelength λ. Letting $\lambda = 2L$ in their results yields the solid curve of Figure 10. Surprisingly, the trends compare favorably for the range of values of 2a/L provided in Reference 3, even though the two cases are considerably different. The results of Sih and Loeber[3] appear to provide a conservative upper bound for 2a/L < 0.40. As 2a/L increases beyond this the results of Mal[7] indicate that the dynamic stress-intensity factor due to a harmonic wave oscillates, and, therefore, for larger 2a/L the harmonic wave results would bear little resemblance to the case discussed here.

The stress pulse used in this experiment, it is believed, approximates the waves due to hypervelocity impact, and, therefore, the results may be of considerable practical use in explaining fractures and spallation due to hypervelocity impact. Particularly, Kinslow[9] has reported that fracture of plexiglas lags the peak stress; this could be explained by the stress-intensity factor lag of peak stress.

CONCLUSIONS

For a dilatational stress pulse the crack tip stress intensity response has been determined. The results show that the stress-intensity factor lags the applied stress and that the maximum stress-intensity factor depends on the crack length to wavelength ratio. Notably, the stress-intensity factor may be 20% larger than the static value for a certain 2a/L and considerably smaller than the static value for other values of 2a/L.

The author wishes to emphasize the qualitative rather than the quantitative results. The method used here did not permit great accuracy; a number of assumptions were employed, measurements were made on fringes hard to see near the crack tip, and results were extrapolated. Nevertheless, the qualitative information and the trends described here are believed to be valid and new.

ACKNOWLEDGMENTS

The author wishes to acknowledge the work of Professor Donald Williams in setting up and operating the dynamic polariscope and the encouragement and suggestions of Professor Ray Kinslow, Head, Department of Engineering Science, Tennessee Technological University. This research was supported by NASA Grant NGR 43-003-007.

REFERENCES

1. Loeber, J. F. and Sih, G. C., "Diffraction of Anti-plane Shear Waves by a Finite Crack," The Journal of the Acoustical Society of America, 44 (1), 90-98 (1968).

2. Sih, G. C. and Loeber, J. F., "Normal Compression and Radial Shear Waves Scattering at a Penny-Shaped Crack in an Elastic Solid," The Journal of the Acoustical Society of America, 46 (3), 711-721 (September, 1969).

3. Sih, G. C. and Loeber, J. F., "Wave Propagation in an Elastic Solid with a Line of Discontinuity or Finite Crack," Quarterly of Applied Mathematics 27 (2), 193-213 (July, 1969).

4. Sih, G. C. and Loeber, J. F., "Interaction of Horizontal Shear Waves with a Running Crack," Journal of Applied Mechanics, Series E, 37 (2), 324-330 (June, 1970).

5. Ravera, R. J. and Sih, G. C., "Transient Analysis of Stress Waves Around Cracks under Anti-plane Strain," The Journal of the Acoustical Society of America, 47 (3), 875-881 (March, 1970).

6. Jahanshahi, A., "A Diffraction Problem and Crack Propagation," Journal of Applied Mechanics, 100-103 (March, 1967).

7. Mal, A. K., "Interaction of Elastic Waves with a Penny-Shaped Crack," International Journal of Engineering Science, 8, 381-388 (May, 1970).

8. Sih, G. C., "Some Elastodynamic Problems of Cracks," International Journal of Fracture Mechanics, 1 (1), 51-68 (1968).

9. Kinslow, R., "Observations of Hypervelocity Impact of Transparent Plastic Targets, AEDC-TDR-64-49, (May, 1964).

10. Miles, J. W., "Homogeneous Solutions in Elastic Wave Propagation," Quarterly of Applied Mathematics, 18 (1), 37-59 (April, 1960).

11. Flitman, L. M., "Waves Caused by a Sudden Crack in a Continuous Elastic Medium," Journal of Applied Mathematics and Mechanics, 27 (4), 938-953 (1963) (Translation of the Soviet Journal Prikladnaia Matematika I Meknanika).

12. Smith, D. G. and Smith, C. W., "A Photoelastic Evaluation of the Influence of Closure and Other Effects Upon the Local Bending Stresses in Cracked Plates," International Journal of Fracture Mechanics, (in press) (1970).

13. Durelli, A. J. and Riley, W. F., Introduction to Photomechanics, Prentice-Hall, Inc., Englewood Cliffs, N. J., p. 355 (1965).

14. Dally, J. W. and Riley, W. F., "Stress Wave Propagation in a Half-Plane Due to a Transient Point Load," Developments in Theoretical and Applied Mechanics, 3, Pergamon Press, New York, 357-377 (1967).

15. Saha, S. "Investigation of Stress Waves in a Half-Plane by Dynamic Photoelasticity," M. S. Thesis, Tennessee Technological University, (April, 1969).

16. Wells, A. A. and Post, D., "The Dynamic Stress Distribution Surrounding a Running Crack--A Photoelastic Analysis," Proc. SESA XXVI (1), 69-92 (1958).

17. Stock, T. A. C., "Stress Field Intensity Factors for Propagating Brittle Cracks," International Journal of Fracture Mechanics, 3 (2), 121-129, (June, 1967).

18. Bradley, W. B. and Kobayashi, A. S., "An Investigation of Propagating Cracks by Dynamic Photoelasticity", Experimental Mechanics, 10 (3), 106-113 (March, 1970).

19. Kinslow, R. and Delano, B., "Stress Waves in Sandwich Plates," TTU-ES-70-3, Research Report, Tennessee Technological University, (August, 1970).

20. Smith, D. G. and Smith, C. W., "Photoelastic Determination of Mixed Mode Stress Intensity Factors," Presented at the Fourth National Symposium on Fracture Mechanics, August 24-26, 1970, at Carnegie-Mellon University, Pittsburgh, Pennsylvania.

LIST OF FIGURES

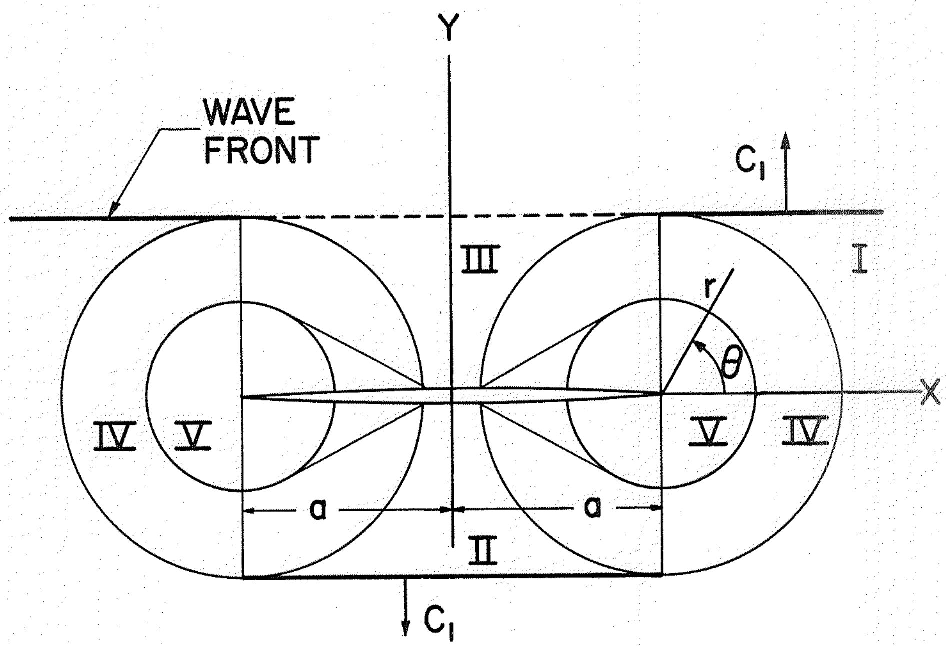

Figure 1. Diffraction of a dilatational pulse by a finite crack for normal incidence

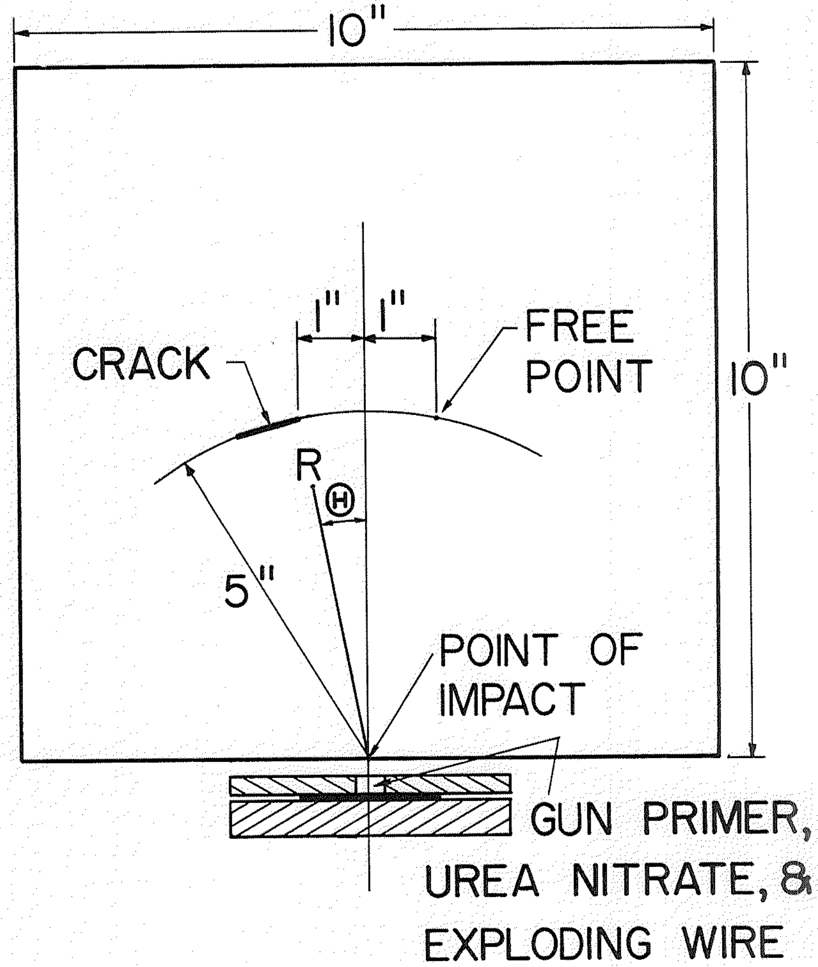

Figure 2. Incident wave and plate geometry

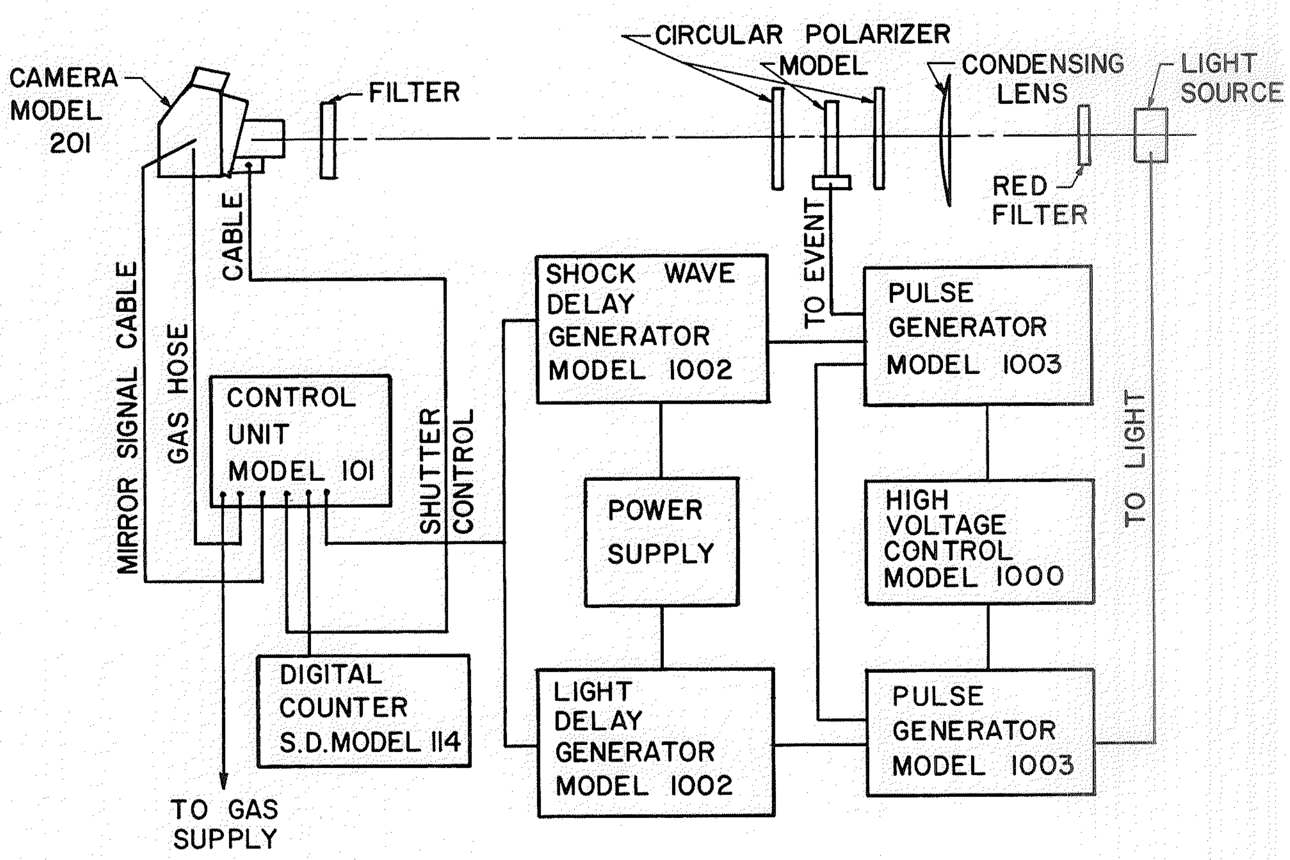

Figure 3. Polariscope, camera, and controls

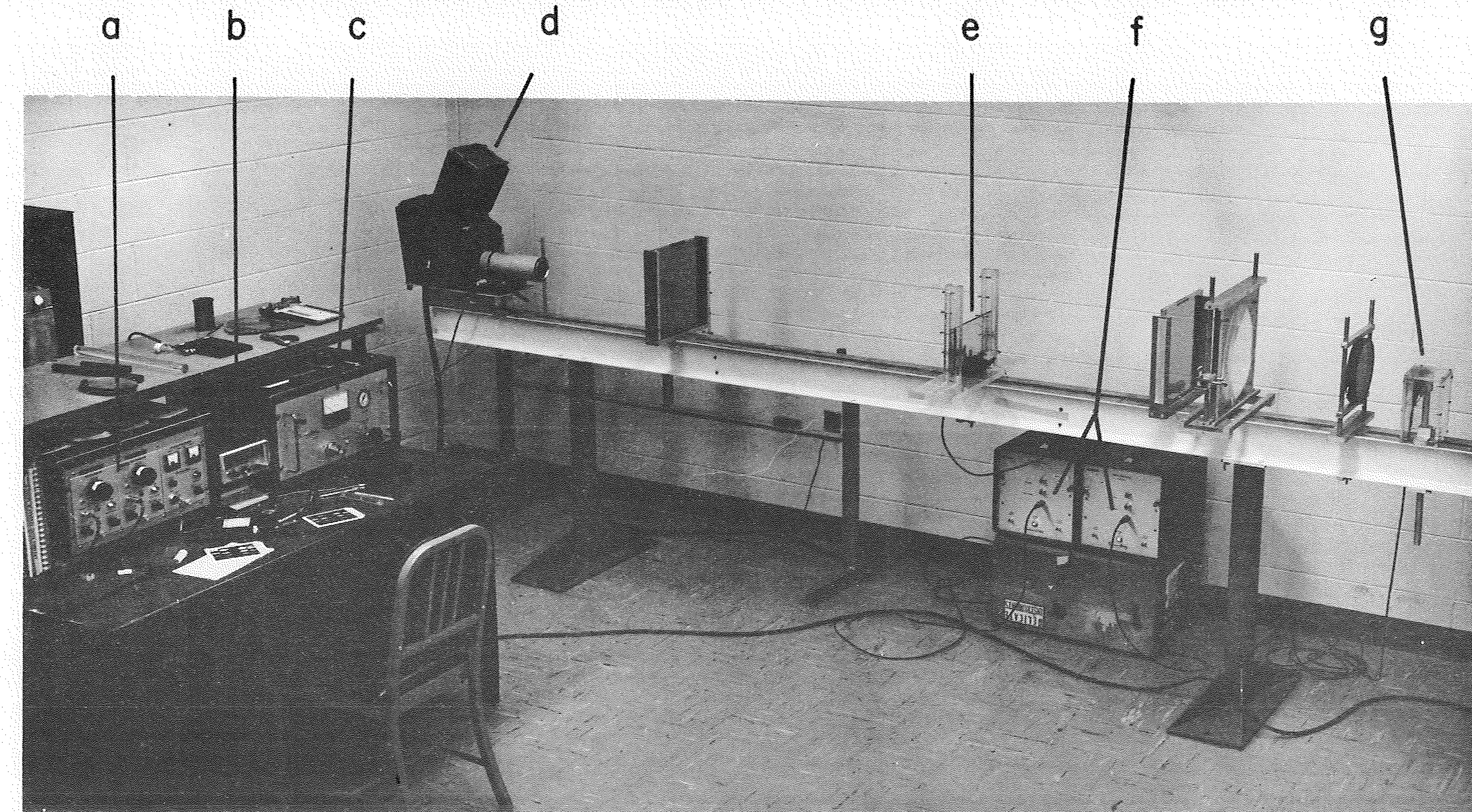

Figure 4. Experimental apparatus. a--light and shock wave delay generators, b--digital counter, c--control unit, d--camera, e--model, f--pulse generators, g--light source.

Figure 5. Light field isochromatics during passage of the stress wave for the 1 inch crack

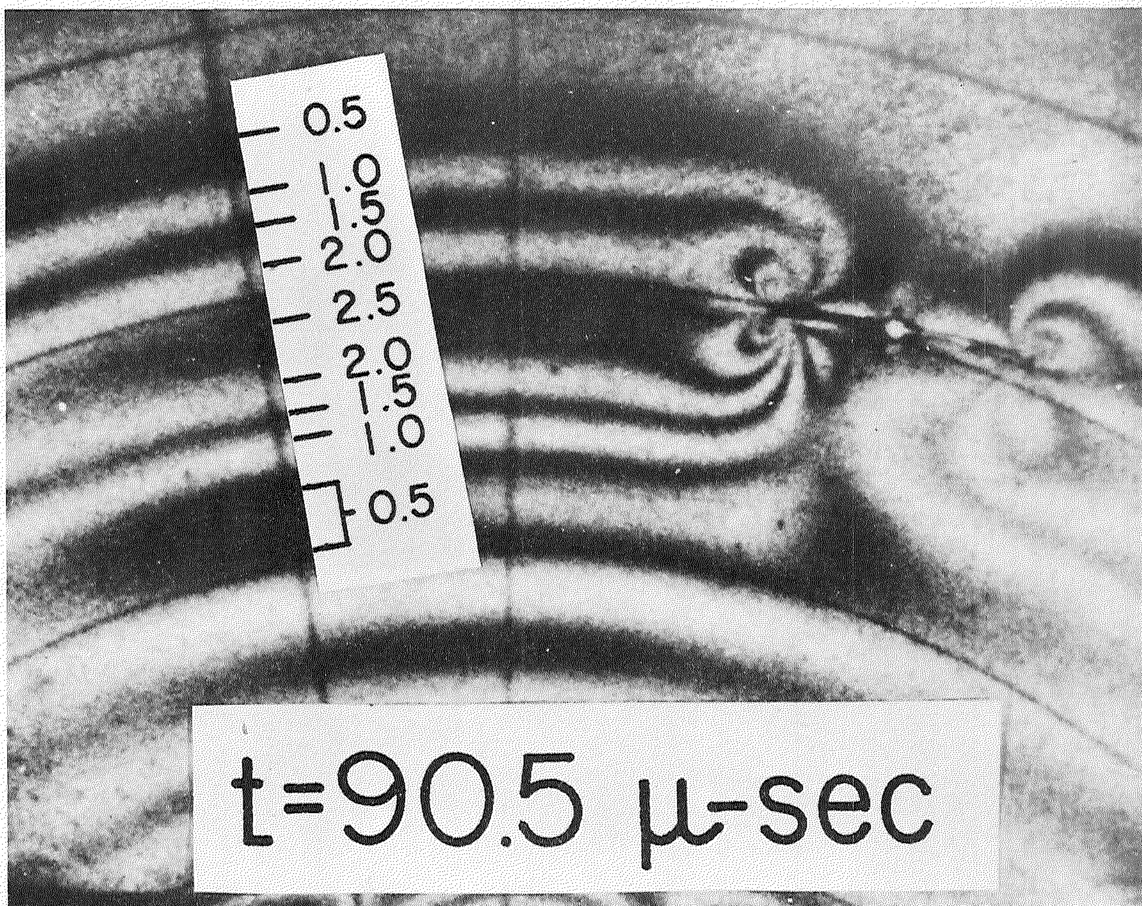

Figure 6. The crack-tip fringes and the incident fringe orders for the 1 inch crack

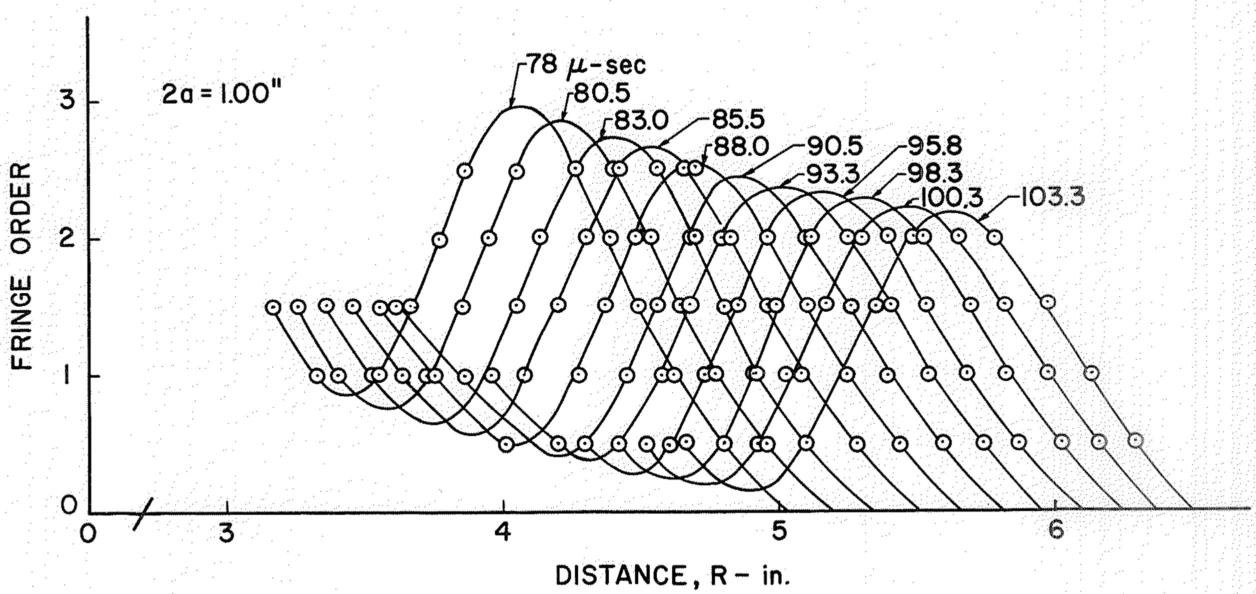

Figure 7. Variation of incident fringe order along a radial line through the free point for various times after the impact

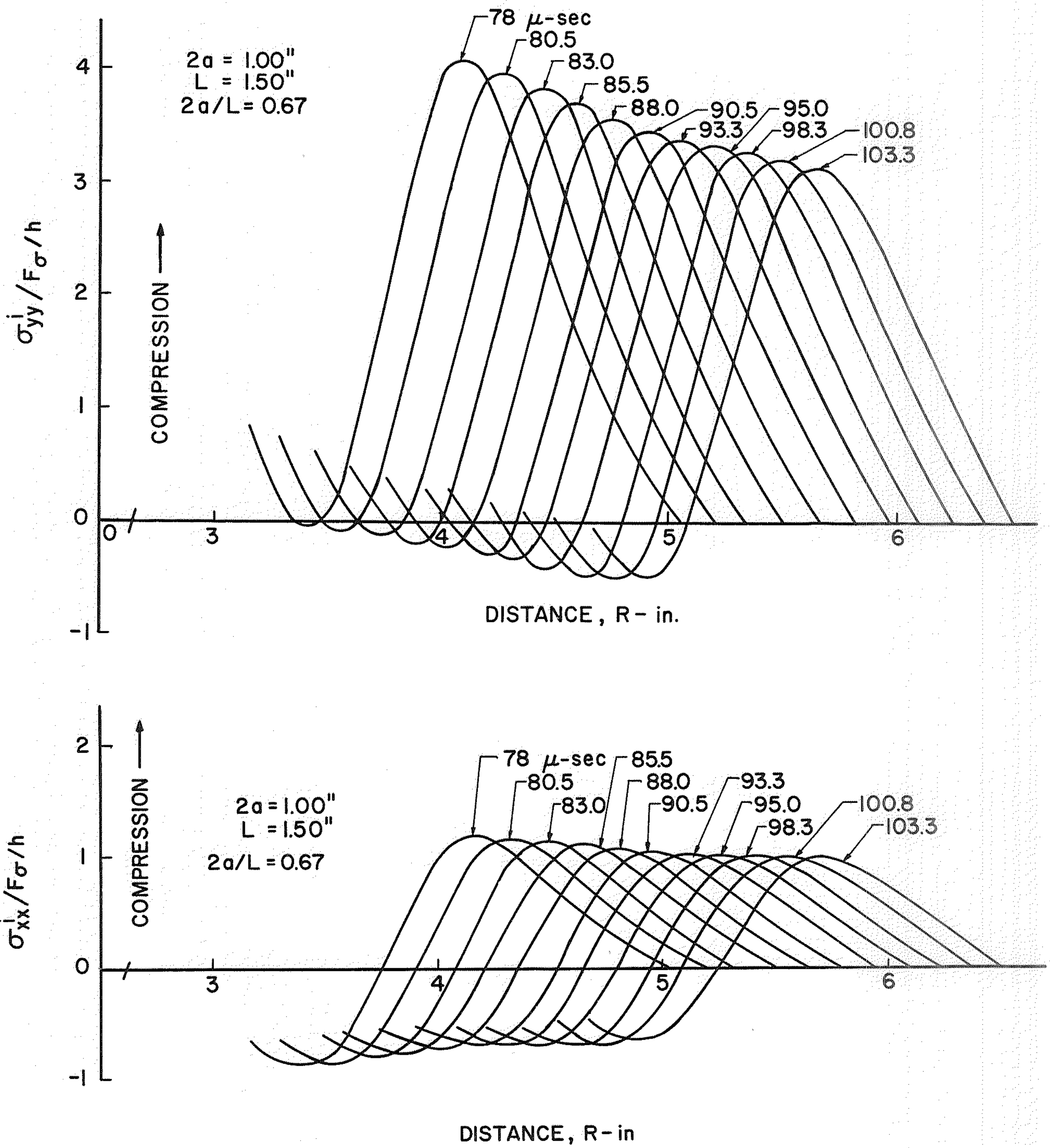

Figure 8. The shape of the incident stress pulse

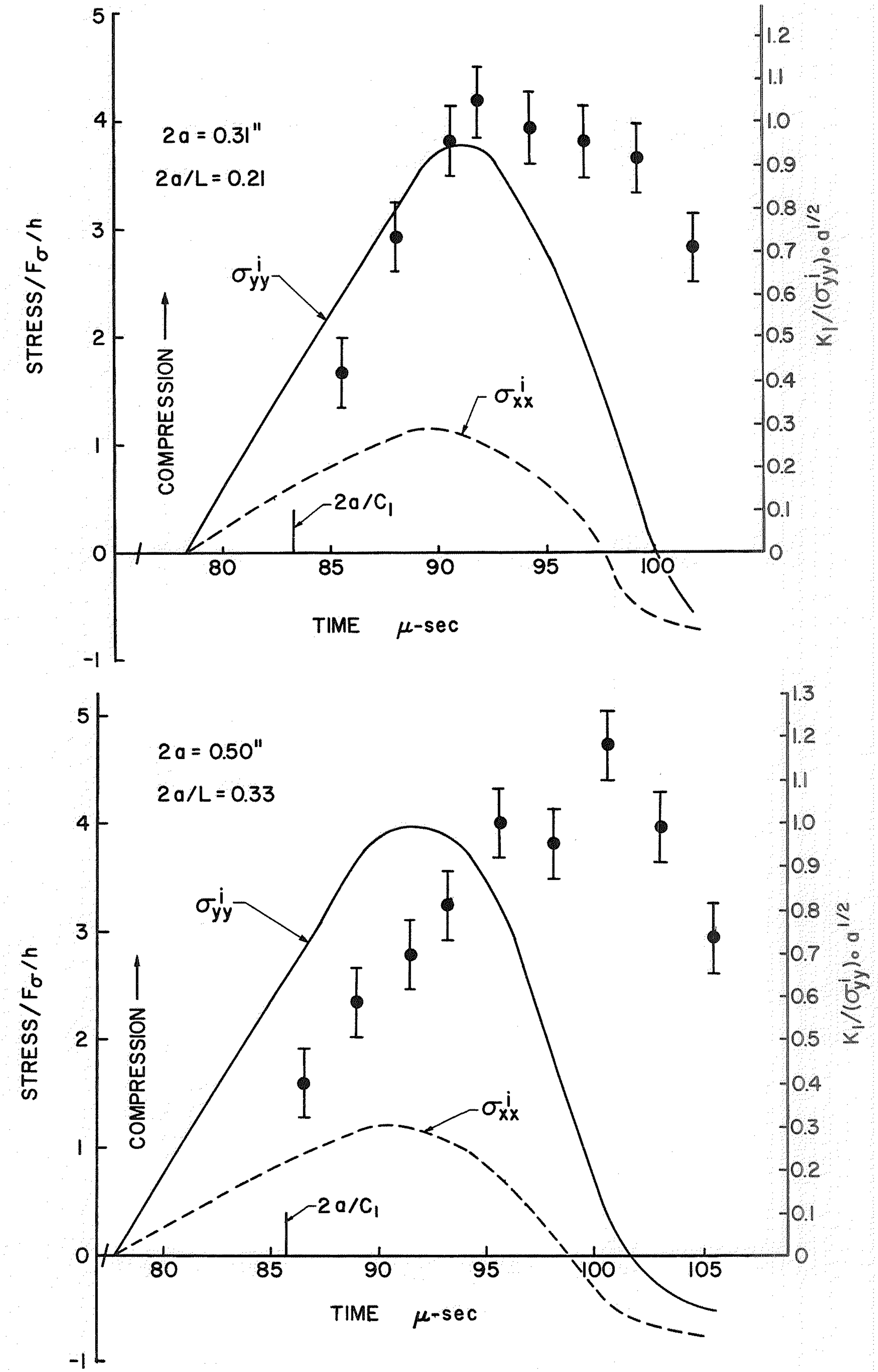

Figure 9. The dynamic stress-intensity factor and crack loading history

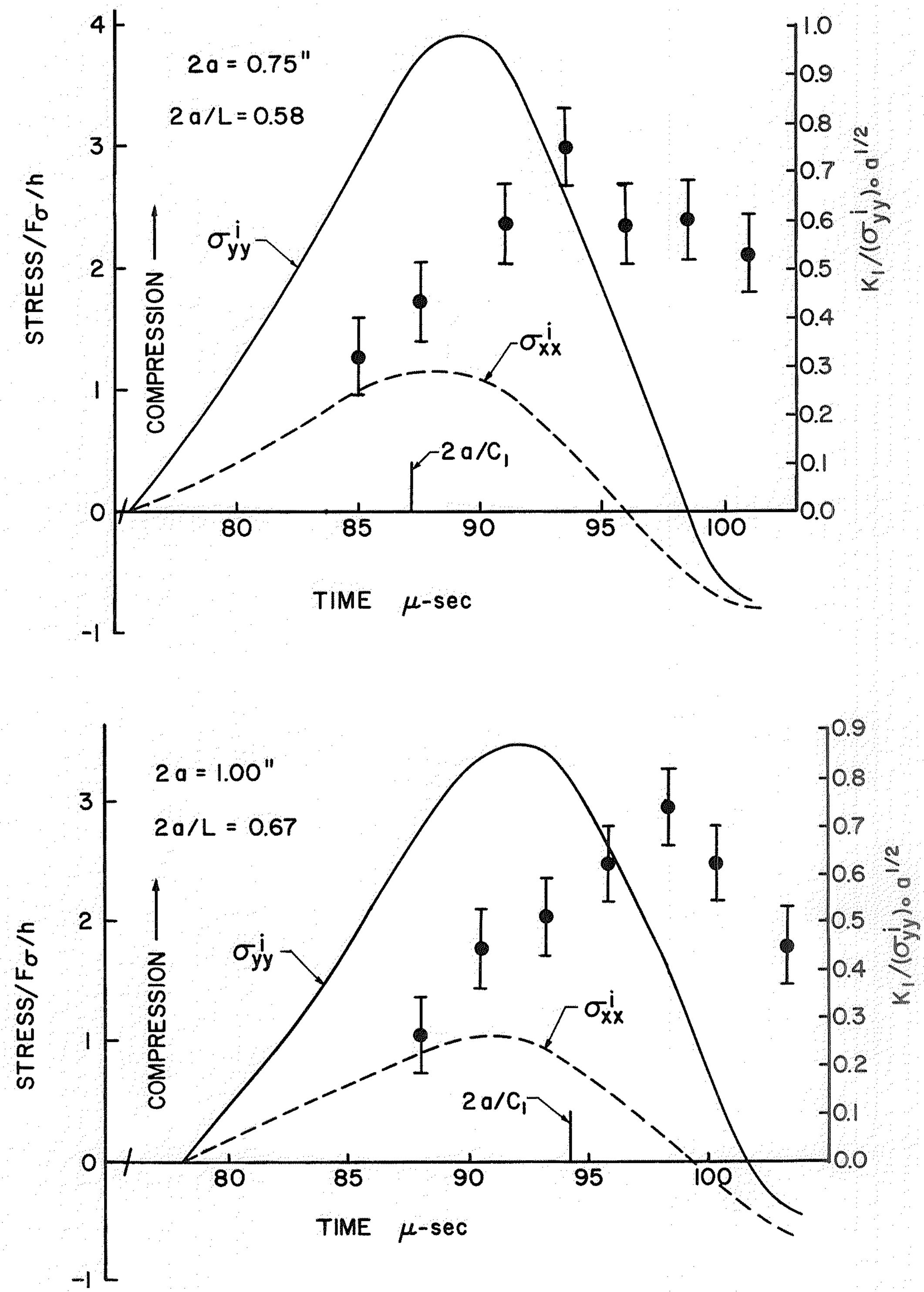

Figure 9. Continued

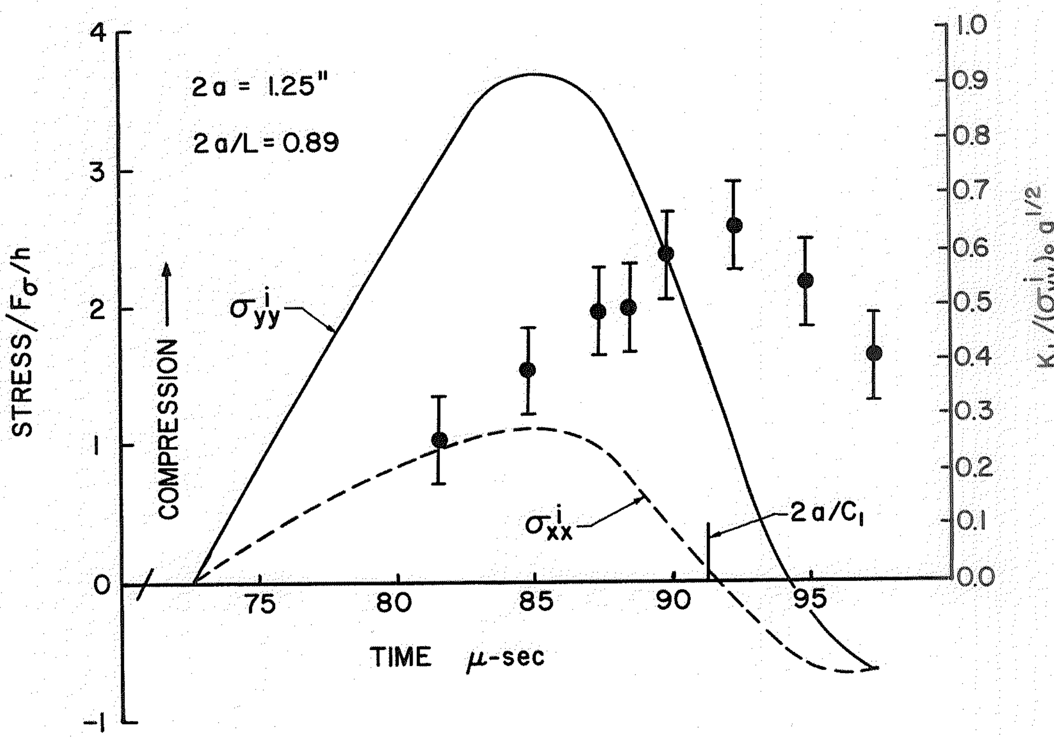

Figure 9. Concluded

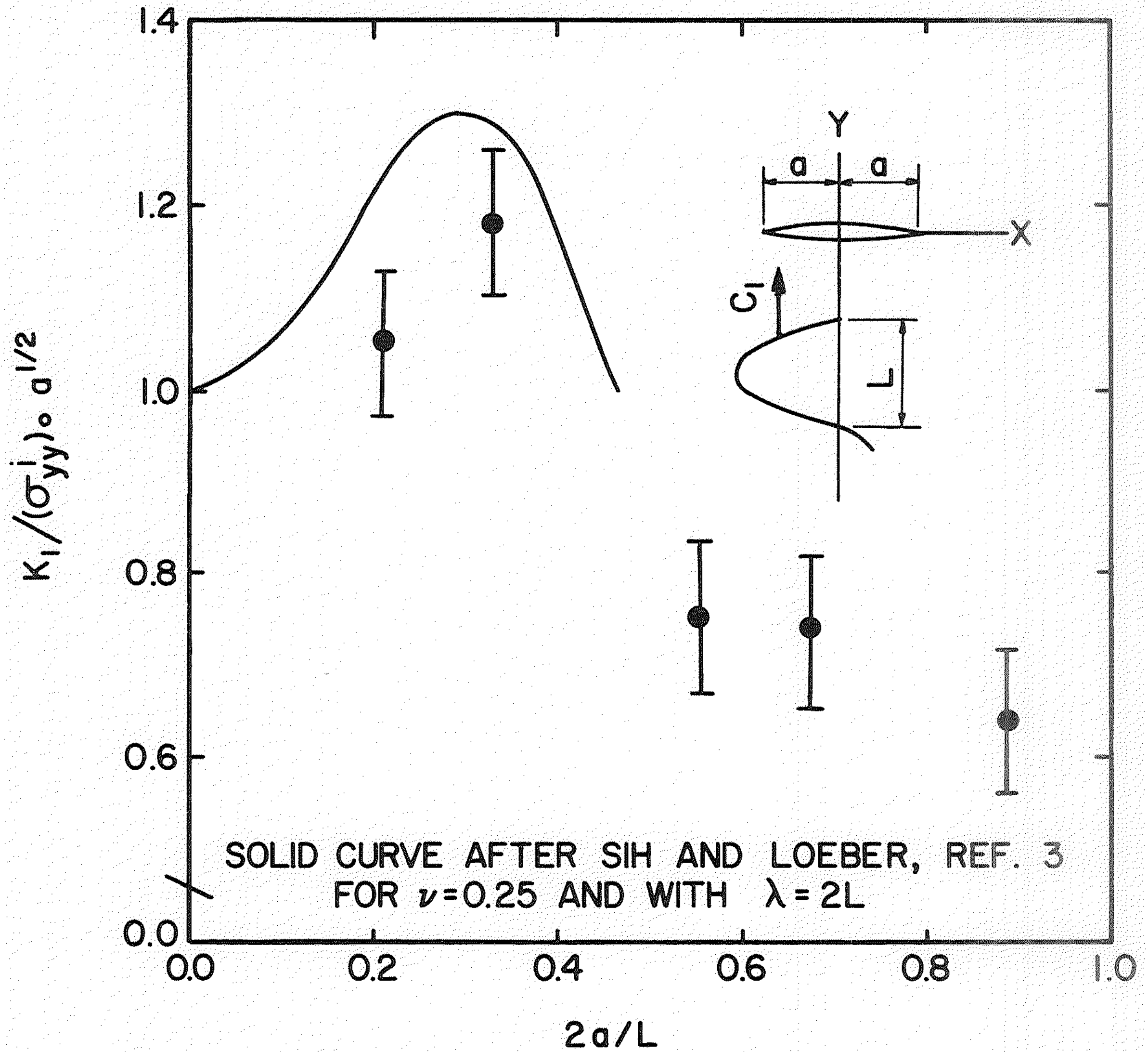

Figure 10. The effect of crack length to pulse length ratio on the maximum stress-intensity factor